

A Prefix Based Approach for Joint Doppler and Channel Estimation in Underwater Communication

Vijay Singh Bhadouria (✉ vsbhadouria@gmail.com)

IIT Delhi: Indian Institute of Technology Delhi <https://orcid.org/0000-0002-2370-3783>

Monika Agrawal

IIT Delhi: Indian Institute of Technology Delhi

Ritesh Kumar

IIT Delhi: Indian Institute of Technology Delhi

Research Article

Keywords:

Posted Date: September 20th, 2022

DOI: <https://doi.org/10.21203/rs.3.rs-739437/v2>

License: © ⓘ This work is licensed under a Creative Commons Attribution 4.0 International License.

[Read Full License](#)

A Prefix Based Approach for Joint Doppler and Channel Estimation in Underwater Communication

Vijay Singh Bhadouria^{1*}, Monika Agrawal² and Ritesh Kumar¹

^{1*}Bharti School of Telecommunication Technology and Management, Indian Institute Of Technology Delhi, 110016, India.

²Centre For Applied Research in Electronics, Indian Institute Of Technology Delhi, 110016, India.

*Corresponding author(s). E-mail(s): vsbhadouria@gmail.com;

Contributing authors: maggarwal@care.iitd.ac.in; riteshkumar1512@gmail.com;

Abstract

Developing a reliable and robust underwater acoustic communication system is a difficult task, due to the complicated nature of the underwater channel, non-stationary noise, and a number of other factors. Indeed, channel estimation or equalization presents numerous challenges in this non-stationary, highly Doppler, multipath environment; as a result, traditional equalizers and PLL-based methods have limited performance. Generally, communication over such time-varying channels is accomplished via packets that contain a prefix/preamble signal for training, a payload containing the actual data, and a silent period for proper alignment. The prefix signal must be designed properly because it is used to estimate the channel and also to determine the start of packet. This paper proposes a novel prefix signal based on the hyperbolic chirp signal, where its Doppler invariance properties enable the extraction of the entire packet even when Doppler and severe multipath are present. Additionally, this proposed prefix enables an efficient and accurate method for fully characterising an underwater channel. The proposed prefix signal is used to estimate the multipath delay and amplitude, and different Doppler scales. Extensive simulations using various channel models are used to determine the proposed method robustness and efficacy under a wide range of conditions. Additionally, the proposed algorithm has been validated on a real-world channel.

1 Introduction

Using acoustics signals as carrier is the best possible way to communicate underwater specially for long ranges. Even after research of so many decades establishing a reliable link of few km at rate of few kbps is very hard task, much more challenging than radio frequency (RF) based wireless air communication [1, 2]. It is mainly because of the complex nature of acoustic channel and harsh noise characteristics [3, 4]. Signal

attenuation increases with the frequency [5]. The low sound speed deteriorates the quality of communication due to the Doppler and large delay spread. The presence of time-varying multipath due to the movement of the transmitter, receiver, and floating boundaries, debris or scatterers make underwater channel much more difficult [6]. Various multipath give different Doppler [7]. Acoustic communication is generally feasible at lower frequencies, i.e., tens of kHz, with limited transmission bandwidth. A few kHz of bandwidth is

categorised as the wideband transmission [8, 9], resulting in the frequency selective channel [10]. In fact, underwater acoustic channels are both frequency and time selective [11], hence termed doubly selective channel [12]. In wideband communication, Doppler spread mainly causes time dilation/compression of received signals and offsets the carrier frequency [13].

These frequency selective channels are handled by various methodologies among them most effective ones are as using highly trained equalizers [14, 15], or by dividing complete frequency selective channel into small orthogonal flat fading channel, (i.e. orthogonal frequency division multiplexing (OFDM)) [16–18], or using well designed orthogonal codes for transmission, i.e., code division multiple access [19] and other specialised techniques. Each technique has its own merit and demerit.

Communication in the doubly selective, non-stationary channel is preferably carried out by transmitting the information in packet form [20]. The size of the packet is generally kept less than that of the coherence time of the channel. Each packet generally contains three fields, i.e. header termed as prefix/preamble, silent period and data. The header is the known signal utilized for frame detection, synchronization and channel estimation [21]. To a large extent, the choice of prefix signal depends upon the channel and in turn the estimation accuracy of the channel depends upon the properties of the prefix signal [22]. For underwater acoustic communication it is required that the prefix signal used should be Doppler tolerant [23]. Various types of prefix signal like pseudo-random bit sequence (PRBS) and linear/hyperbolic frequency modulation (LFM/HFM), has been used in literature for channel sounding [24, 25]. Two LFM chirp signals, i.e. up chirp and down chirp in tandem are used to capture the time-varying information, i.e. Doppler scale of the channel [25]. Packet using [26] two signals at the head and tail end of packet i.e. prefix and postfix has also been suggested. The disadvantage of these methods is that both the chirp signals are separated in time. Therefore, the channel both signals might be different. Moreover two signals, in turns, puts a limit on the data rate. To overcome this issue a single prefix to jointly estimate Doppler scale and channel is proposed in [27], though it do not compromise with data rate, but the estimation error

increases with the increase in Doppler.

The presence of Doppler makes channel estimation a arduous task. Subspace based methods [26] are more effective with lower Doppler, whereas, compressive sensing-based methods are more effective when channel has sparse structure and large Doppler offset. Multi-channel adaptive DFE [28] based equalizer is an effective way to track and equalize. In fact, many algorithms for estimating the channel for various scenario has been proposed e.g.in different kind of noise [29], in the presence of carrier and timing offset. Deep neural network framework has also been used [30] for channel estimation and correction. But a generic method to reliably estimate/equalize underwater channel is an open problem due to non-stationary, highly Doppler, multipath environment.

In this paper, we design an appropriate prefix signals for UWA communication environment. A single prefix-based packet structure for underwater communication has been thoroughly investigated. Further unique properties of the prefix signal assist us in developing novel and robust joint Doppler and channel estimation technique. Proposed method not only estimate the channel in the presence of Doppler, but it also estimates Doppler scales and delay parameters for various multipath. A two-stage algorithm provides a coarse estimate first, then refines it using lookup tables. Extensive numerical simulation studies demonstrate the efficacy of the proposed frame structure and channel estimation algorithm in various simulated and real-world environments.

2 Proposed Frame Structure

The acoustic underwater communication channel is very complex; therefore, both prefix and postfix [31], as shown in Fig. 1 are primarily used for channel estimation, packet extraction, synchronization etc. This channel usually varies rapidly [5], hence, it limits the use of this type of packet structure. One possible way of handling is by reducing the size of the packet s.t. the channel remains stationary for the entire packet duration. However, this will reduce the effective data rate. To circum-



Fig. 1 Conventional Frame Structure

Prefix	Guard	Data	Guard
--------	-------	------	-------

Fig. 2 Suggested Frame Structure

vent this, a single prefix-based packet, as shown in Fig. 2 has been suggested. The packet contains a guard band, one prefix signal and payload. The suggested design provides a better effective data as it has only one prefix signal as compared to the earlier design, therefore will be used for all its merits. Further, the choice of prefix is also crucial, as this will be responsible for equalizing multipath, combating the Doppler and performing synchronization. The packet structure, prefix signal and the system algorithm to handle the tough underwater channel is unfolded in the following section.

2.1 Prefix Selection

The good prefix signal should have following features,

- The autocorrelation function of the prefix signal should be close to impulse function, with a low side lobe level and small main lobe width.
- It should be robust for Doppler induced scaling, ideally it should be Doppler invariant.
- High Doppler resolution, i.e., small Doppler frequency should be resolvable.
- High temporal resolution, i.e., all multipath should be resolvable.
- The compression or expansion of the prefix signal should be analytically expressed.

Pseudo-random bit sequence (PRBS) and linear/hyperbolic frequency modulation (LFM/HFM) are used as prefix signal. The PRBS are very sensitive towards the Doppler based scaling. Whereas LFM and HFM signals are less sensitive to Doppler scaling, therefore, can be potential candidates for prefix signal in underwater communication. We further study these signals and their properties to understand their fitment in this underwater communication.

3 Design of Prefix Signal

3.1 LFM and HFM signal

LFM signal with frequency support of $[f_0, f_T]$ is expressed as,

$$l(t) = \begin{cases} \cos(2\pi f_0 t + \pi b_l t^2) & 0 \leq t \leq T \\ 0 & \text{otherwise} \end{cases} \quad (1)$$

where, b_l is the chirp rate, $\frac{f_T - f_0}{T}$, indicates the rate of change of frequency, f_T denotes the highest and f_0 denotes the lowest frequency and T is time duration. HFM signal with the same frequency and time support is given as,

$$s_H(t) = \begin{cases} \cos\left(\frac{-2\pi}{b} \log(1 - b f_0 t)\right) & 0 \leq t \leq T \\ 0 & \text{otherwise} \end{cases} \quad (2)$$

where, $b = \frac{f_T - f_0}{f_T f_0 T}$ is the chirp rate. The first role of prefix signal is the detection of the start of the packet; the received signal is correlated with the transmitted prefix, correlation peak gives the start of the packet. The accuracy of detection depends upon the autocorrelation properties of the prefix signal. These properties can be studied using autocorrelation and wideband ambiguity function (WAF) with bandwidth (B), time duration (T) and their product, commonly known as bandwidth-time product, i.e. BT, as crucial design parameters. The main performance metrics for the autocorrelation function are the width and height of the main lobe for the given energy signal. Ideally, the impulse type autocorrelation function provides the best multipath delay resolution, i.e. theoretically, all arrival paths can be resolved. Wideband ambiguity function (WAF) incorporates Doppler scaling; therefore, it is used to study correlation properties in Doppler. We study these performance metrics for both prefix signals under various conditions to understand and compare their behaviour.

3.2 Auto Correlation Function

Autocorrelation function of signal $s(t)$ is defined as:

$$R(\tau) = \int (s(t)s^*((t - \tau))) dt \quad (3)$$

It is symmetric function about $\tau = 0$, with peak value of $R(0)$. The width of the main lobe of $R(\tau)$

is a measure of delay resolution. 3-dB main lobe width τ_{3dB} can be evaluated as:

$$\tau_{3dB} = \tau_{max} - \tau_{min} \quad (4)$$

where, τ_{max} and τ_{min} are the maximum and minimum value delay corresponding half power point can be obtained as solution of the equation $R(\tau) = \frac{R(0)}{2}$ respectively. Fig. 3 shows the impact of bandwidth (B) on autocorrelation for LFM and HFM signal. It can be observed from Fig. 3 that, for a given energy of the signal, the increase in bandwidth reduces the width of the main lobe of autocorrelation function, which provides better delay resolution.

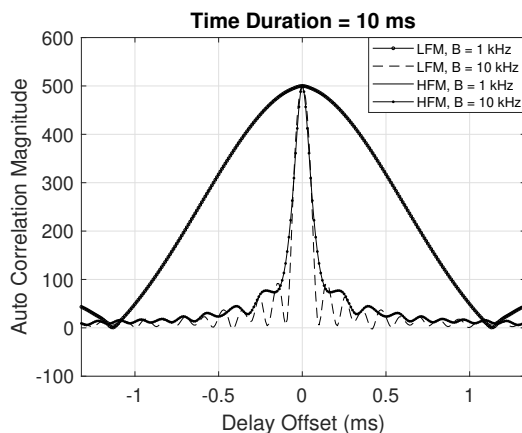


Fig. 3 Impact of increasing BT by changing the bandwidth of signal

For getting a better understanding, τ_{3dB} is evaluated for various values of bandwidth (B) normalized to the fixed center frequency, As depicted in Fig. 4. the main lobe of the LFM signal is narrower than that of the HFM, and the difference increases with increase in bandwidth. The main lobe width can be easily measured in terms of root mean square (rms) bandwidth in terms given by,

$$B_{rms} = 2 \sqrt{\frac{\int_{f_0}^{f_T} (f - f_0)^2 |S(f)|^2 df}{\int_{f_0}^{f_T} |S(f)|^2 df}} \quad (5)$$

where, $S(f)$ is the frequency response of signal. The plots of the rms bandwidth of both the LFM and the HFM signal is shown in Fig. 5. It can be observed that for higher bandwidth, i.e

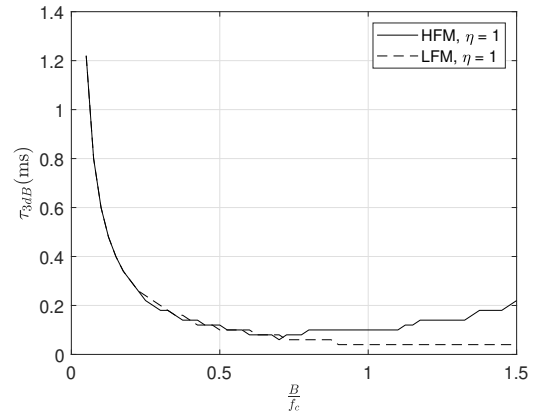


Fig. 4 Auto correlation plot for HFM and LFM signal

10 kHz, the LFM signal has larger rms bandwidth than that of the HFM signal, while for lower bandwidth, i.e. 1 kHz, both the signals has similar rms bandwidth. Therefore, the LFM signal has a narrower main lobe than that of the HFM signal and as bandwidth increases, the LFM signal provides better delay resolution than the HFM signal. Autocorrelation properties quantify

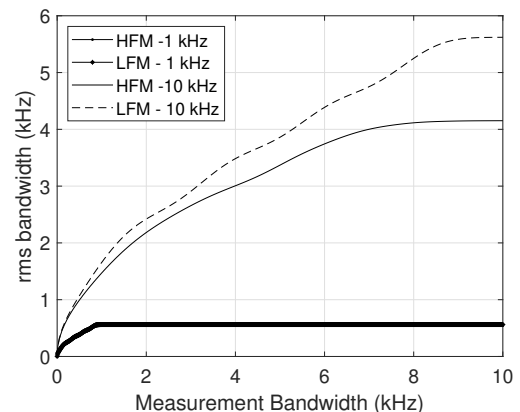


Fig. 5 RMS bandwidth comparison of LFM and HFM signal

the prefix signal performance only for the case of no or almost negligible Doppler. To analyze the impact of Doppler on correlation properties, we investigate the wideband ambiguity function in detail.

3.3 Wideband Ambiguity Function

Doppler is more prevalent in underwater communication, therefore, plays an important role in the prefix design. The impact of Doppler is being studied using the wideband ambiguity function (WAF) [32]. It models the Doppler effect on the wideband signal by time scaling, i.e., dilation. Mathematically, WAF, $\chi(\eta, \tau)$, of signal $s(t)$ is given by:

$$\chi(\eta, \tau) = \sqrt{\eta} \int (s(t)s^*(\eta(t - \tau)))dt \quad (6)$$

where τ time delay and η Doppler induced scaling. It can easily be seen that,

$$\chi(\eta, \tau) \leq \chi(1, 0) \quad (7)$$

Normalized WAF is defined as: $\chi_N(\eta, \tau) = \frac{\chi(\eta, \tau)}{\chi(1, 0)}$. To analyse the impact of Doppler on LFM and HFM signal, we have studied WAF for under different conditions and scenario. The details of the parameters and scenarios, which are chosen to get comprehensive overview are given in Table 1.

Shape, width and span of 3 dB WAF con-

Table 1 Prefix Signal Test Cases

Case I	B=1 kHz ,T=1 ms, BT=1
Case II	B=10 kHz ,T=10 ms, BT=100
Case III	B=1 kHz ,T=10 ms, BT=10
Case IV	B=10 kHz ,T=1 ms, BT=10
Sampling Frequency	100kHz
Centre Frequency	20kHz

tours obtained by solving the equation $\chi_N(\eta, \tau) = \frac{1}{2}$, depicts the important characteristics of prefix signal. Shape tells the nature of the overall impact of the Doppler. Width quantifies delay and Doppler resolution, while span depicts the inherent Doppler tolerance. For lower value of BT , i.e. $BT = 1$ and $BT = 10$, the 3dB WAF contours as shown in Fig. 6 of both LFM and HFM signals are almost linear strip passing through the origin ($\eta = 1, \tau = 0$), completely overlaps. On the other hand, for $BT = 100$, WAF contour of LFM signal is linear, but for HFM signal it is curved i.e. the ridges of the contour varies slowly, which provides better insensitivity to the Doppler scale. Hence, the HFM signal has better Doppler tolerance than

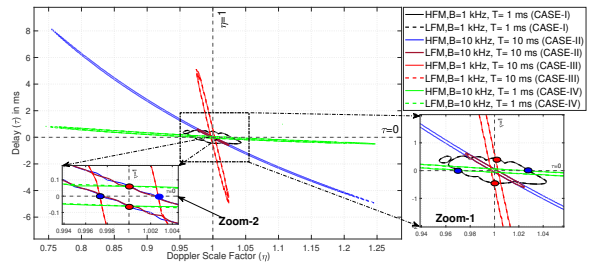


Fig. 6 Wideband ambiguity function for LFM and HFM signal for various bandwidth (B) and time duration (T) values. Zoom-1 is the zoomed plot to show the delay resolution, i.e. difference between two red dots, and the Doppler scale resolution, i.e. difference between two blue dots, for Case I, Case III and Case IV. Zoom-2 is the zoomed plot shown for same purpose as zoom-1, except that it is for comparing Case II, Case III and Case IV.

that of the LFM signal for larger BT values.

From Zoom plot 1 of Fig. 6, it can be seen that when $BT = 100$, 3 dB WAF contour of LFM signal is smaller than that of the HFM signal, hence, LFM signal incurs more SNR loss with Doppler scaling than HFM signal. Therefore, LFM signal is more sensitive to Doppler-induced scaling than HFM signal for higher BT values. Further, for delay resolution is quantified using, τ_{3dB} , which is measured as the distance between the points of intersection of WAF ($\chi_N(\eta, \tau)$) and line $\eta = 1$. In Fig. 6 these points of intersection are shown by two red dots in the zoom plot 1 and zoom plot 2. It can be observed from zoom plots 1 and 2 that delay resolution for Case II and Case IV is the same but better than Case I and Case III. It is due to the increase in bandwidth B , i.e., from $1kHz$ to $10kHz$.

Similarly the Doppler resolution (η_{3dB}), can be obtained by measuring the distance between the point of intersection of WAF with the line $\tau = 0$, indicated by the two blue dots shown in zoomed plots. Doppler resolution for Case II and Case III is approximately equal, and it is better than that of Case I and Case IV due to the increase in time duration from $1ms$ to $10ms$.

The delay resolution for various Doppler scales can also be obtained by measuring the main lobe width of WAF for the given Doppler scale η . To get a better understanding Fig. 7 plots WAF for two different values of Doppler scale factors i.e., $\eta = 1$ and $\eta = 0.95$ for $\frac{B}{f_c} = 0.5$. For the Doppler scale of 0.95, the main lobe for both LFM and HFM signal is shifted, also the delay resolution of

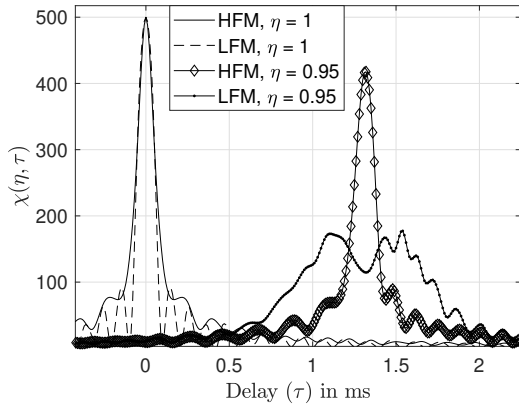


Fig. 7 Impact of Doppler scaling on LFM and HFM signals at $\frac{B}{f_c}$

the LFM signal becomes poorer due to the widening of the main lobe of correlation output. Further Fig. 8 plots the delay resolution, i.e., τ_{3dB}^η as a function of normalized bandwidth for $\eta = 0.95$ and $\eta = 0.99$, normalized bandwidth is evaluated by measuring the distance between two half-power points of the main lobe. For lower bandwidth, both LFM and HFM have similar performance; as bandwidth increases, delay resolution of LFM tends to become poor and HFM performs better. Another critical parameter is the peak value of the ambiguity function; with Doppler scale the peak value of the ambiguity function decreases. This effect is more prominent in the case of LFM than HFM signal. It shows that the HFM signal is more robust than the LFM signal under the Doppler effect.

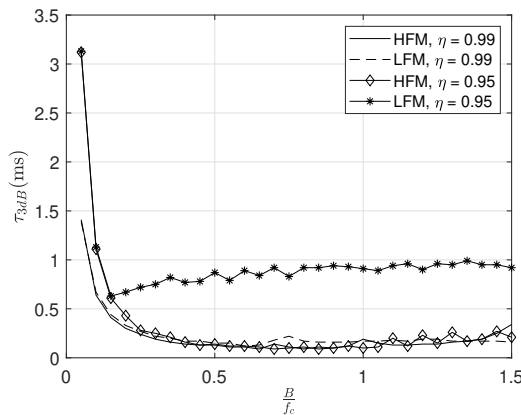


Fig. 8 Delay resolution of LFM and HFM signal under Doppler effect

Further, the available signal processing capacity for given Doppler scale factor η , can also be quantitatively measured using,

$$L(\eta) = -10 \log \chi_N(\eta, 0). \quad (8)$$

The higher the value of $L(\eta)$ lesser will be its Doppler tolerance, the Doppler-induced scaling reduces processing gain due to a mismatch in the transmitted and the received signal. Fig.9 plots $L(\eta)$ for various scale factors, it can be observed that for LFM signal $L(\eta)$ increases rapidly with a slight increase of Doppler scale, whereas HFM signal have marginally less loss, only 3 dB loss with Doppler scale changing from 0.8 to 1.2.

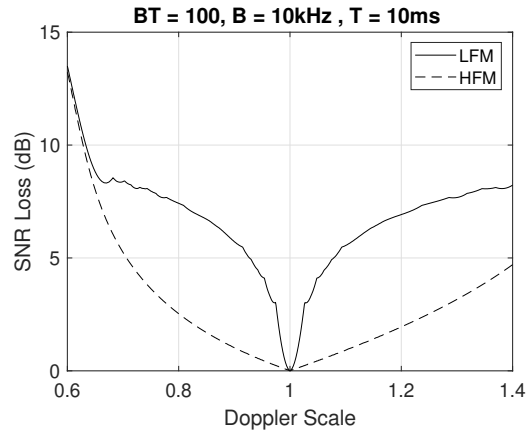


Fig. 9 SNR Loss with respect to Doppler induced scaling for $BT=100$

3.4 Receiver Operating Characteristics(ROC)

As these prefix signals are used to detect the packet and receiver operating characteristics (ROC), which plots the probability of detection (PD), which plots the probability of false alarm (PFA), is a gold standard metric to study detection. ROC under different scenarios described in Table 2 for parameters given in Table 3 for both LFM and HFM are being studied. The observations are summarised below:

- On increasing the bandwidth 5kHz to 10 kHz robustness to Doppler scaling for HFM improves, whereas for the LFM signal it reduces with an increase in bandwidth.

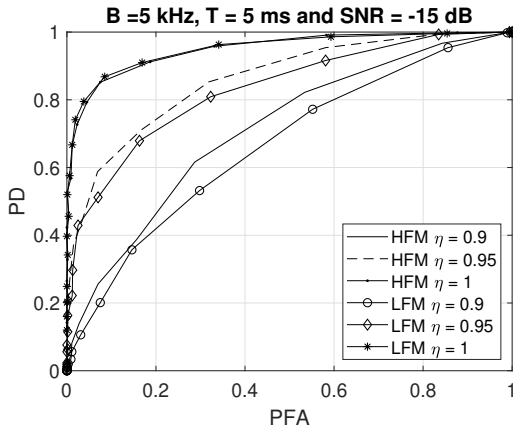
Table 2 Cases of ROC simulation

Case I	$B=5 \text{ kHz}, T=5 \text{ ms}$
Case II	$B=5 \text{ kHz}, T=10 \text{ ms}$
Case III	$B=10 \text{ kHz}, T=5 \text{ ms}$
Case IV	$B=10 \text{ kHz}, T=10 \text{ ms}$

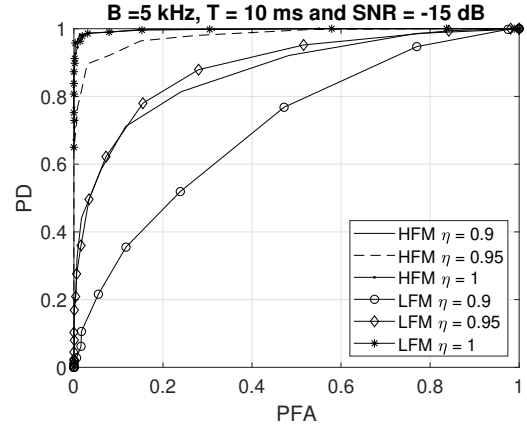
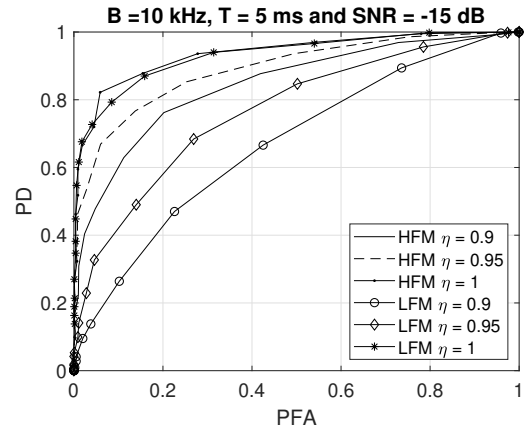
- With the decrease of T , both the LFM signal and the HFM signal performance deteriorate. It is due to the reduction in the processing gain because of less time.

Table 3 Simulation parameters

Sr. No.	Parameter	Value
1	Bandwidth	1 kHz, 10 kHz
2	Sampling Frequency	100 kHz
3	Centre Frequency	20 kHz
4	Signal Duration	1 ms, 10 ms
5	Doppler Scale Factor	0.9, 0.95 and 1
6	Number of Simulation	10,00,000
7	SNR	-15 dB

**Fig. 10** ROC curve for LFM and HFM of various Doppler Scale values- Case I

It can be observed from the ROC curve that, though in the absence of the Doppler effect, i.e., $\eta = 1$, both the signals have equivalent performance. However, the performance of the LFM signal degrades as compared to that of HFM as the Doppler effect increases. Another important result is summarized in this lemma.

**Fig. 11** ROC curve for LFM and HFM of various Doppler Scale values- Case II**Fig. 12** ROC curve for LFM and HFM of various Doppler Scale values- Case III

Lemma 1 *HFM signals are invariant to Doppler induced scaling due to its hyperbolic type time-frequency coupling, whereas LFM signals are affected by Doppler induced scaling.*

Proof The proof is given in Appendix A.

The summary of the analysis done above is given in Table 4, which shows the clear advantage of using the HFM signal over the LFM signal. A large Doppler spread characterizes UWA channel; hence, it is expected that the transmitted signal will undergo a significant Doppler scaling effect. As per the above discussion, the HFM signal is more suitable under such conditions of the UWA channel.

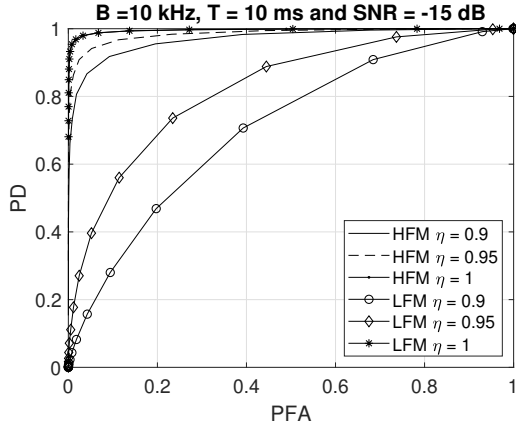


Fig. 13 ROC curve for LFM and HFM of various Doppler Scale values- Case IV

Table 4 Comparison of LFM and HFM signal

Parameter	LFM	HFM
Doppler Scale and delay Resolution (without Doppler effect)	Better	Poor
Doppler Scale and delay Resolution (with Doppler effect)	Poor	Better
SNR Loss with Doppler effect	Poor	Better
Detection Performance (ROC) (with Doppler effect)	Poor	Better

4 Doppler and Delay Estimation

As discussed HFM signal is Doppler insensitive for various reasons, especially for larger BT values. Therefore, in our work, the HFM signal is used as a prefix signal. Estimation of Doppler, Delay and channel is essential for reliable communication. HFM signal not only is good candidate for prefix signal but also can be used in estimation of Doppler, delay, and channel estimation. One important property of HFM signal is elaborated using the following Lemma.

Lemma 2 *The effect of Doppler-induced scaling in an HFM pulse can be modeled as a linear time shift. Doppler scaled HFM signal, i.e., $s(\eta(t - \tau))$ can be modeled as linear time shift in the HFM signal $s(t)$, such that:*

$$s(\eta(t - \tau)) = s(t - \Delta t) \quad (9)$$

where, linear time shift, i.e. Δt , is given by:

$$\Delta t = \tau \pm \frac{1 - \eta}{\eta b f_0} \quad (10)$$

where, τ is the propagation delay of the path, f_0 is the start frequency of the chirp, and η & b is the Doppler scale factor and the chirp rate respectively.

Proof given in Appendix A.

This relation can simply be used to estimate the delay and Doppler scale induced i.e. τ and η . Time shifts Δt corresponding to different HFM signals with same time and frequency support can simultaneously be solved to estimate η and τ . Same time support is required to avoid the impact of time variation of the channel in delay and Doppler estimation. Frequency support of the signals should cover the entire available bandwidth of the channel for its complete characterization. The best possible two HFM signals are up-chirp HFM and down-chirp HFM supported over the entire bandwidth [27]. To provide the same time support and avoid channel variability, we use the linear combination of these up-chirp HFM and down-chirp HFM signals given as,

$$s(t) = s_u(t) + s_d(t) \quad (11)$$

where, $s_u(t)$ is unit power normalised up chirp HFM and $s_d(t)$ is unit power normalised down chirp HFM given as,

$$s_u(t) = \begin{cases} \frac{1}{\sqrt{2}} \cos\left(\frac{-2\pi}{b} \log(1 - b f_0 t)\right) & 0 \leq t \leq T \\ 0 & \text{otherwise} \end{cases} \quad (12)$$

$$s_d(t) = \begin{cases} \frac{1}{\sqrt{2}} \cos\left(\frac{2\pi}{b} \log(1 + b f_T t)\right) & 0 \leq t \leq T \\ 0 & \text{otherwise} \end{cases} \quad (13)$$

From Lemma 2 linear time shift Δt_u between transmitted and received up chirp HFM under the effect of Doppler scaling η are given as:

$$\Delta t_u = \tau + \frac{1 - \eta}{\eta b f_0}. \quad (14)$$

Similarly linear time shift Δt_d for down chirp HFM is given as,

$$\Delta t_d = \tau - \frac{1 - \eta}{\eta b f_T}. \quad (15)$$

5 Channel Estimation Algorithm

Underwater channels are time varying in nature, the output of the linear time-variant channel, i.e., $r(t)$ can be given as,

$$r(t) = \int h(\tau, t - \tau) s(\tau) d\tau + w(t) \quad (16)$$

where, $h(\tau, t)$ is the time-varying channel impulse response, $s(t)$ be the transmitted signal, τ is the propagation path delay, and $w(t)$ be the additive noise. Propagation of signal in the underwater acoustic medium is manifested by various phenomena like scattering, refraction, and reflection. The time-varying impulse response $h(\tau, t)$ can be modeled as,

$$h(t, \tau) = \sum_{i=1}^L \sqrt{\eta_i} A_i(t) \delta(t - \tau_i(t)) \quad (17)$$

where, $A_i(t)$ and $\tau_i(t)$ are the time-varying amplitude and delay corresponding to i^{th} multipath. Let L be the number of multipath. The time-varying delay corresponding to i^{th} multipath for the case of constant relative velocity between transmitter and receiver can be approximated as:

$$\tau_i(t) = \tau_i(0) + a_i t \quad (18)$$

where, $\tau_i(0)$ is fixed time delay and a_i is the rate of change of i^{th} multipath delay. Substituting, (18) and (17) in (16), we get:

$$r(t) = \sum_{i=1}^L \sqrt{\eta_i} A_i(t) s(\eta_i(t - \tau_i)) + w(t) \quad (19)$$

where, $\tau_i = \frac{\tau_i(0)}{\eta_i}$ and $\eta_i = 1 - a_i$. The received signal $r(t)$ can be modeled as the summation of paths with propagation delay τ_i with corresponding Doppler scale η_i . This can be seen as multi-scale multi-lag (MSML) type of channel i.e. different Doppler scaling and correspondingly different delay for each multipath. Here the task of channel estimation boils down to the determination of three parameters, i.e., the amplitude (A_i), the propagation delay (τ_i), and the Doppler scale factor (η_i) for significant number of multipath. It can be accomplished by 2D search over each Doppler scale and delay dimension, but that will be costly in terms of complexity. The complexity of the search algorithm can also be reduced by reducing the number of dimensions to be searched.

Again hyperbolic time-frequency coupling of HFM signal is used to reduce the search dimension by one order, making it 1D search. Two stage algorithm consisting of coarse and fine joint Doppler scale and delay estimation is formulated. The coarse estimation employs a correlation-based method while fine estimation is based on a look-up table (LUT) based search to estimate these parameters.

5.1 Coarse Doppler Estimation

Complete flow of the proposed coarse channel estimation method is shown in Fig. 14. It uses a correlation-based approach to estimate the delay between the transmitted and the received signal. Correlator output is used by the peak detection algorithm for the detection of true peaks. Peak detection algorithm annihilates false peaks to get true estimate. Delays associated with the estimated peaks are used to jointly estimate the associated path's Doppler scale and propagation delay.

5.2 Correlation Based Detector

Received signal $r(t)$ is correlated with the transmitted up chirp, i.e., $s_u(t)$. Correlator output can be

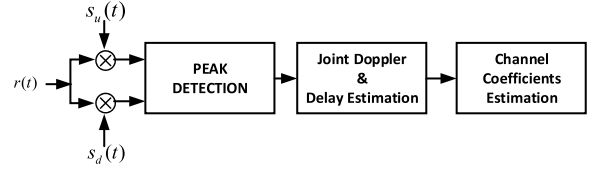


Fig. 14 Block Diagram of Proposed Coarse Channel Estimation Algorithm

expressed as:

$$\hat{g}_u(\tau', t) = \int_0^{T+T_g} r(t) s_u(t - \tau') dt \quad (20)$$

where, T is the duration of prefix signal and T_g is the guard interval. On substituting (19) in (20), we get:

$$\hat{g}_u(\tau', t) = \int_0^{T+T_g} \sum_{i=1}^L \sqrt{\eta_i} A_i s(\eta_i(t - \tau_i)) s_u(t - \tau') dt + w'(t) \quad (21)$$

where, $w'(t) = \int_0^{T+T_g} w(t) s_u(t - \tau') dt$, after rearrangement,

$$\hat{g}_u(\tau', t) = \sum_{i=1}^L \sqrt{\eta_i} A_i R(\eta_i, \tau_i - \tau') + w'(t) \quad (22)$$

where, $R(\eta_i, \tau_i - \tau') = \int_0^{T+T_g} s(\eta_i(t - \tau_i)) s_u(t - \tau') dt$. Using (11), it can be expressed as:

$$R(\eta_i, \tau_i - \tau') = R_{uu}(\eta_i, \tau_i - \tau') + R_{du}(\eta_i, \tau_i - \tau') \quad (23)$$

where, $R_{uu}(\eta_i, \tau_i - \tau') = \int_0^{T+T_g} s_u(\eta_i(t - \tau_i)) s_u(t - \tau') dt$ and $R_{du}(\eta_i, \tau_i - \tau') = \int_0^{T+T_g} s_d(\eta_i(t - \tau_i)) s_u(t - \tau') dt$.

The proposed prefix consists of a summation of up and down HFM chirps due to orthogonality of up and down HFM chirp, we get:

$$R_{uu}(\eta_i, \tau_i - \tau') \gg R_{du}(\eta_i, \tau_i - \tau')$$

Therefore

$$R(\eta_i, \tau - \tau') \approx R_{uu}(\eta_i, \tau - \tau') \quad (24)$$

putting (24) in (22), we get:

$$\hat{g}_u(\tau', t) = \sum_{i=1}^L \sqrt{\eta_i} A_i R_{uu}(\eta_i, \tau_i - \tau') + w'(t) \quad (25)$$

In ideal scenario, $R_{uu}(\eta_i, \tau_i - \tau')$ is an impulse function, i.e., $R_{uu}(\eta_i, \tau_i - \tau') \approx \delta(t - \tau_i)$ and in the absence of Doppler effect, from (17) and (25), we can deduce that $\hat{g}_u(\tau', t) \approx h(\tau, t)$. Moreover, the peaks of $\hat{g}_u(\tau', t)$ are strictly at propagation delay τ_i . Therefore, at any time instance t , the channel impulse response, i.e. $h(\tau, t)$, can be estimated by observing the peaks of $\hat{g}_u(\tau', t)$. However, as a result of Doppler scaling η_i , as per (14), the position of the peaks will

be shifted from τ_i to $\Delta t_{u,i}$, shifted peak position is given by:

$$\Delta t_{u,i} = \tau_i + \frac{1 - \eta_i}{\eta_i b f_0}. \quad (26)$$

Furthermore, the corresponding magnitude of the peak is given by:

$$p_{u,i} = \sqrt{\eta_i} A_i R_{uu}(\eta_i, \Delta t_{u,i}) \quad (27)$$

Similarly, the output of the correlator with down chirp HFM can be expressed as:

$$\hat{g}_d(\tau', t) = \sum_{i=1}^L \sqrt{\eta_i} A_i R_{dd}(\eta_i, \tau_i - \tau') + w''(t) \quad (28)$$

where, $w'(t) = \int_0^{T+T_g} w(t) s_d(t - \tau') dt$ and $R_{dd}(\eta_i, \tau_i - \tau') = \int s_d(\eta_i(t - \tau_i)) s_d(t - \tau') dt$. Position of peaks for $\hat{g}_d(\tau', t)$, i.e. correlator output for corresponding to down chirp HFM can be expressed as:

$$\Delta t_{d,i} = \tau_i - \frac{1 - \eta_i}{\eta_i b f_T}. \quad (29)$$

where, f_T is the start frequency of down chirp, the magnitude of the corresponding peak is given by:

$$p_{d,i} = \sqrt{\eta_i} A_i R_{dd}(\eta_i, \Delta t_{d,i}) \quad (30)$$

It can be observed that in (25) and (28), the correlator output corresponding to up chirp and down chirp HFM are not same, i.e. $\hat{g}_u(\tau', t) \neq \hat{g}_d(\tau', t)$, this is mainly due to Doppler. This can be more effectively visualized using the 3 dB contour of WAF Fig. 15. WAF of proposed prefix signal consist of two

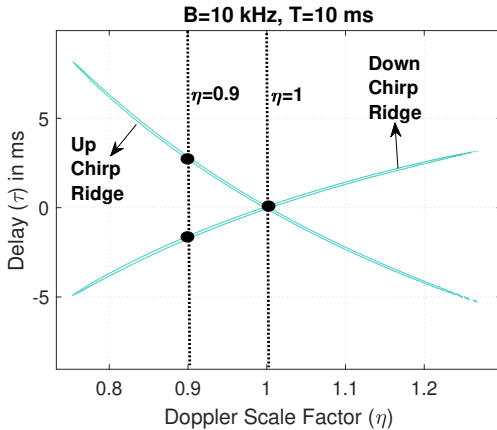


Fig. 15 3 dB contour of WAF for proposed prefix signal, black dots represents intersection of $\eta = \eta_i$ with respective curve

ridges, concave up the ridge for up chirp and concave down the ridge for the down chirp. For given value of Doppler scale, η_i linear time shifts for both up chirp and down chirp are different. It is represented by the

intersection of respective contour by line $\eta = \eta_i$, as shown in Fig. 15 by black dots. Hence, value of η_i and τ_i can be obtained by solving equations (26) and (29) simultaneously. Therefore to estimate the channel, the peaks of the correlation need to be estimated, which is elaborated further.

5.3 Peak Detection

Here signal from the transmitter to the receiver reaches through many paths and as discussed above delay corresponding to each path is estimated by detecting the peaks of the $\hat{g}_u(\tau', t)$. To estimate these peaks and to ascertain that they are true peaks, two-step procedure is proposed in this work. The first step is to keep only those peaks which are greater than a certain threshold p_{Nth} . The value of the threshold p_{Nth} is decided on the targeted false alarm rate. As false peaks are due to large sidelobes, p_{th} is determined using the side lobe level (SLL) of the autocorrelation function of the transmitted prefix signal. Another parameter to ascertain the correct peak ensuring that the time difference between consecutive / nearest two peaks has to be more than the time difference between the main lobe and side lobe of the transmitted prefix signal i.e. N_{th} . Therefore prominent peaks are determined by comparing the magnitude as well as separation between two consecutive peaks, proposed method is described as, Algorithm 1.

After peak detection, next task is to estimate the Doppler and delay using the locations of the peaks.

5.4 Doppler and Delay profile estimation

Delay and Doppler scale estimation described above is used to jointly estimate delay and Doppler of each path. Let the peak amplitude detected for the up chirp and down chirp arranged in $L \times 1$ vectors \mathbf{p}_u and \mathbf{p}_d respectively as,

$$\mathbf{p}_u = [p_{u,1}, p_{u,2}, \dots, p_{u,L}]^T \quad (31)$$

and,

$$\mathbf{p}_d = [p_{d,1}, p_{d,2}, \dots, p_{d,L}]^T. \quad (32)$$

where, $p_{u,i}$ and $p_{d,i}$ are the amplitude of i^{th} correlator peaks corresponding to up chirp and down chirp respectively. and $t_{u,i}$ and $t_{d,i}$ are the corresponding locations and L is number of multipath. Define

$$\mathbf{t}_u = [t_{u,1}, t_{u,2}, \dots, t_{u,L}]^T. \quad (33)$$

$$\mathbf{t}_d = [t_{d,1}, t_{d,2}, \dots, t_{d,L}]^T. \quad (34)$$

Lemma 3 The Doppler scale factor $\boldsymbol{\eta} = [\eta_1, \eta_2, \dots, \eta_L]$ and propagation delay $\boldsymbol{\tau} =$

Algorithm 1 Algorithm for prominent Peak Detection

Correlator output ($\hat{g}_u(\tau', t)$ or $\hat{g}_d(\tau', t)$);

Step 1 : Elimination of false peaks due to noise ;

if $p_{u,i}$ or $p_{d,i} > p_{Nth}$ **then**

 | Go to step 2

else

 | Eliminate the peak

Step 2 : Compare the peak ($p_{u,i}$ or $p_{d,i}$) with two of its immediate neighbouring peaks ($p_{u,i-1}$ or $p_{d,i-1}$ and $p_{u,i+1}$ or $p_{d,i+1}$) **if** $\frac{2p_{u,i}}{p_{u,i-1}+p_{u,i+1}} > p_{th}$

or $\frac{2p_{d,i}}{p_{d,i-1}+p_{d,i+1}} > p_{th}$ **then**

 | Go to step 3

else

 | Eliminate the peak

Step 3 : Calculate the difference between the two consecutive peaks, i.e $\nabla t = \Delta t(u, i) - \Delta t(u, i-1)$ or $\Delta t(d, i) - \Delta t(d, i-1)$; **if** $\nabla t > N_{th}$ **then**

 | Go to step 4

else

 | Eliminate the peak

Step 4: Store the peaks value and their time index in the form of column vector, \mathbf{p} and \mathbf{t} respectively

$[\tau_1, \tau_2, \dots, \tau_L]$, can be jointly estimated using the peak location vector \mathbf{t}_u and \mathbf{t}_d . Estimated $\hat{\boldsymbol{\eta}}$ is given as:

$$\hat{\boldsymbol{\eta}} = \Upsilon^{-1} \mathbf{I} \quad (35)$$

where, $\Upsilon = \text{diag}(\frac{\mathbf{t}_u - \mathbf{t}_d}{T})(\frac{B}{2f_c})$ and \mathbf{I} is a $L \times 1$ vector containing all ones, B is the bandwidth with f_c corresponding center frequency. Estimated propagation delay ($\hat{\boldsymbol{\tau}}$) is given as

$$\hat{\boldsymbol{\tau}} = \frac{\mathbf{t}_u + \mathbf{t}_d}{2} + \frac{T}{2} \Upsilon^{-1} (\boldsymbol{\eta} - 1) \quad (36)$$

where,

$$\boldsymbol{\Gamma} = \text{diag}(\boldsymbol{\eta}) \quad (37)$$

Proof Given in Appendix B

Estimated Doppler and delay estimated from (35) and (36) are coarse. Finer correction to the estimated values is further required to meet desired performance.

5.5 Fine Doppler Scale Correction Method

It can be observed from (35) and (36) that, the value of estimated Doppler scale factor $\hat{\boldsymbol{\eta}}$ depends upon $\mathbf{t}_u - \mathbf{t}_d$. Therefore the resolution of $\hat{\boldsymbol{\eta}}$ depends upon the sampling rate. In other words the estimated Doppler scale $\hat{\boldsymbol{\eta}}$ can take a certain value depending upon the

sampling time T_s . These possible values are, $\tilde{\eta}$ given as,

$$\tilde{\eta} = \begin{cases} \frac{1}{1 \pm \frac{nT_s}{T} \frac{B}{2f_c}} & \eta \neq 1, n \neq 0 \\ 1 & n = 0, \eta = 1 \end{cases} \quad (38)$$

As $t_{u,i} - t_{d,i} \not\approx \pm nT_s$ hence the actual value of Doppler scale will be different from estimated can lie anywhere in the interval, $[\frac{1}{1 \pm \frac{nT_s}{T} \frac{B}{2f_c}}, \frac{1}{1 \pm \frac{(n+1)T_s}{T} \frac{B}{2f_c}}]$ and quantization error will not uniform. The non-uniformity of Doppler scale limits the joint Doppler scale and delay estimation algorithm. It may result in raised noise floor at higher SNR. To address this issue, we propose a novel look-up table (LUT) based method. The process flow of the proposed algorithm is given in Algorithm 2. Using the coarse estimate of Doppler

Algorithm 2 Fine Doppler scale estimation Process Flow

Step 1 : LUT Formation;

Step 2 : Read the coarse estimated Doppler scale value;

Step 3 : Find index of Doppler value in LUT ;

Step 4 : Micro grid (M) formation with desired Doppler resolution;

Step 5 :

if $\text{size}(M) = 1$ **then**

 | Coarse estimated Doppler value is optimum;

 | Go to step 3;

else

 | Grid search for all values in micro grid; Select the scale value, that has maximum cross correlation with transmitted prefix, as optimum;

 | Go to step 3 ;

with (38) a LUT (39) with possible values of the Doppler scale is formed. Further, the Doppler scale is always limited by relative velocity between source and receiver, i.e., $\frac{2v_{max}}{c}$, where v_{max} is the maximum relative velocity between source and receiver, and c is the velocity of sound in water. It ascertains the upper and lower limit of the Doppler scale.

$$\mathcal{L} = \begin{bmatrix} 1 - \frac{v_{max}}{c} \\ \frac{1}{1 + \frac{nT_s}{T} \frac{B}{f_c}} \\ \vdots \\ \frac{1}{1 - \frac{nT_s}{T} \frac{B}{f_c}} \\ 1 + \frac{v_{max}}{c} \end{bmatrix} \quad (39)$$

The coarse estimated Doppler scale is compared with the entries in \mathcal{L} . Let, j be the index of \mathcal{L} corresponding to the estimated Doppler scale ($\tilde{\eta}_i$), i.e. $\mathcal{L}(j) = \tilde{\eta}_i$. Further the Doppler scale values corresponding to

$(j-1)^{th}$ to $(j+1)^{th}$ entries of \mathcal{L} , are further divided uniformly according to the targeted Doppler scale resolution desired ($\delta\eta$) and define \mathcal{G} as,

$$\mathcal{G} = \begin{bmatrix} \mathcal{L}(j-1) \\ \mathcal{L}(j-1) + \delta\eta \\ \mathcal{L}(j-1) + 2\delta\eta \\ \vdots \\ \mathcal{L}(j-1) + (M-2)\delta\eta \\ \mathcal{L}(j+1) \end{bmatrix} \quad (40)$$

Finally the optimum Doppler scale value is obtained as,

$$\hat{\eta}_i = \underset{i}{\operatorname{argmax}}(\underset{\tau}{\operatorname{argmax}}(\int s_r(\frac{1}{\mathcal{G}[i]}t)s(t-\tau)dt)) \quad (41)$$

The advantage of micro-grid formulation is that the number of entries in micro-grid depends upon the desired resolution $\delta\eta$. Though the above approach looks computation-intensive, this algorithm can run in parallel for each received path; hence, computations can be done in real-time.

5.6 Channel Coefficient Estimation

After delay and Doppler estimation, the next task is to estimate the amplitude of the respective path. The amplitude of the respective path is estimated by correlating the transmitted prefix with the resampled received signal $s_{rr}(t)$, resampled by estimated Doppler scale,

$$s_{rr}(t) = \sqrt{\hat{\eta}_i} r(\frac{t}{\hat{\eta}_i}) \quad (42)$$

where, $\hat{\eta}_i$ is the estimated Doppler scale factor of that particular path. The amplitude of that particular path can be estimated as:

$$\hat{A}_i = R_{rs}(\hat{\tau}_i); \quad (43)$$

where, $R_{rs}(\tau)$ is the correlation of the resampled received signal with the transmitted prefix as,

$$R_{rs}(\tau) = \int s_{rr}(t-\tau)s(t)dt. \quad (44)$$

$\hat{\tau}_i$ is the estimated propagation delay of that multipath, associated with the peak of $R_{rs}(\tau)$.

6 Result and Discussion

6.1 Performance of the proposed algorithm for the delay and the Doppler scale estimation with signal to noise ratio (SNR)

Performance of delay and Doppler estimation algorithm has been evaluated for parameters given in

Table 5 Coarse Doppler Scale Estimation Simulation Parameters

Sr. No.	Parameter Name	Value
1	Centre Frequency (f_c)	14kHz
2	Bandwidth (f_b)	12kHz
3	Sampling Frequency (f_s)	100kHz
4	Time Duration (T)	10ms
5	Doppler scale values (η)	0.8 to 1.2

Table 5. All results are obtained by keeping desired Doppler grid resolution, i.e., $\delta\eta = 1e^{-6}$. The proposed algorithm has been evaluated for four Doppler scale values: $\eta = 0.995, 0.99, 1.001$ and 1.01 . Total number of $1e^4$ Monte Carlo simulations are used for the performance evaluation. Estimation error for the Doppler scale factor (η_i), propagation delay (τ_i), and the channel amplitude are evaluated by using the following relationships:

$$\hat{\psi}_i^\eta = \frac{1}{N_{mc}} \sum_{m=1}^{N_{mc}} [|\hat{\eta}_{i,m} - \eta_i|^2] \quad (45)$$

$$\hat{\psi}_i^\tau = \frac{1}{N_{mc}} \sum_{m=1}^{N_{mc}} [|\hat{\tau}_{i,m} - \tau_i|^2] \quad (46)$$

$$\hat{\psi}_i^A = \frac{1}{N_{mc}} \sum_{m=1}^{N_{mc}} \left[\left| \frac{\hat{A}_{i,m} - A_i}{A_i} \right|^2 \right] \quad (47)$$

where, $\hat{\psi}_i^{(\cdot)}$ is the estimation error.

The results of both Doppler scale and delay estimation have been shown in Fig. 16 and Fig. 17 respectively. The proposed algorithm is compared with the wavelet-based channel estimation suggested in [27]. It can be observed from figures that the performances of proposed Doppler scale estimation method outperforms the method proposed in [27] by orders of magnitude, except for the Doppler scale value of $\eta = 1.01$, in this case, the performance improvement is marginal at low SNR. Similarly, the delay estimation using the proposed method also performs significantly better than that of [27]. The Doppler estimation error at $\eta = 0.995$ is best, which provides much better estimate of the channel as shown in Fig. 18 for the given Doppler scale resolution of $\delta\eta = 1e^{-6}$. Better Doppler scale and delay estimation have resulted in more accurate channel estimation.

6.2 Performance of channel estimation with SNR

Further channel estimation performance has been evaluated for BELLHOP [33] channel simulated on MATLAB, as shown in Fig. 19, with parameters given in Table 6. The performance of the Doppler scale and

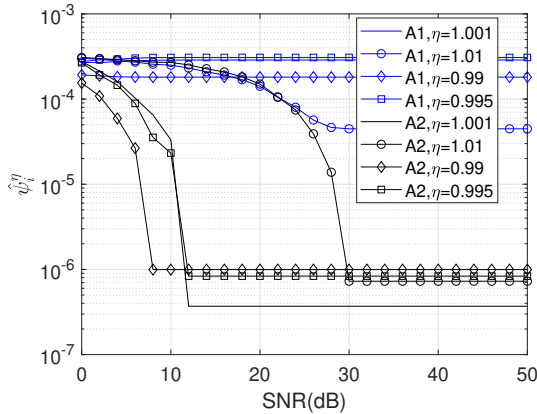


Fig. 16 Performance comparison for Doppler scale estimation; A1: wavelet based algorithm [27], A2 : proposed algorithm.

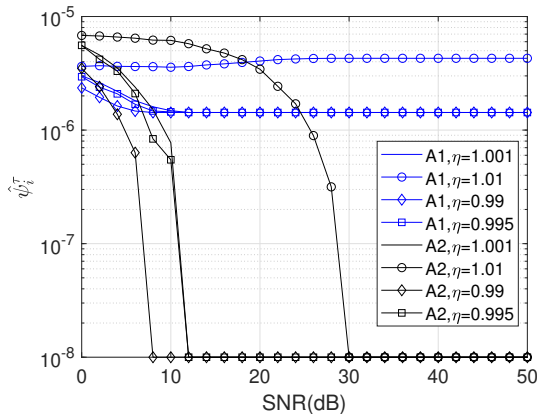


Fig. 17 Performance comparison for delay estimation; A1: wavelet based algorithm [27], A2 : proposed algorithm.

delay estimation algorithm is given in Fig. 20, it shows the performance of the proposed algorithm is superior to the wavelet based method [27]. The result is shown in Fig. 22, which shows that the channel estimation error of the proposed algorithm is much lesser than that of the wavelet-based method mainly for SNR greater than 10 dB. The proposed algorithm can be tuned to the desired Doppler resolution. It, in turn, makes channel estimation more robust and provides better estimation results at higher SNR.

7 Conclusion

A correlation-based algorithm for estimating MSML type UWA channel has been proposed. Firstly, the

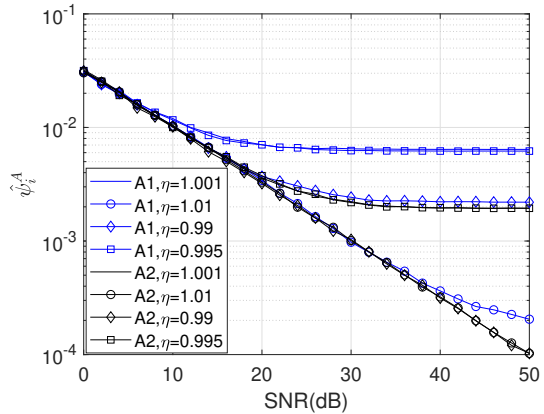


Fig. 18 Performance comparison for channel estimation; A1: wavelet based algorithm [27], A2 : proposed algorithm.

Table 6 Channel and Prefix Signal Parameters

Parameter Name	Value
Centre Frequency (f_c)	14kHz
Bandwidth (f_c)	12kHz
Sampling Frequency (f_s)	100kHz
Transmitter height (ht)	20 m
Receiver height (hr)	50 m
Water Column height (hw)	60 m
Transmitter & Receiver Separation (d)	500 m
Transmitter Horizontal Velocity (v)	6 m/s
Number of paths	3
Absorption Coefficient	0.98,0.8,0.7
Bandwidth-Time Product (BT) of signal	120

HFM and the LFM signals are compared as a potential candidates of prefix. HFM, because for various reasons, has been chosen. Further Doppler insensitive methods to estimate the delay and Doppler scale have been suggested. It has lead to a robust channel estimation algorithm. Simulation results both on the simulated BELLHOP channel and otherwise show the superiority of the proposed algorithm.

Declaration

All authors declare that they have no conflicts of interest.

References

- [1] Qiao G, Babar Z, Ma L, Liu S, Wu J. MIMO-OFDM underwater acoustic communication systems—A review. *Physical Communication*. 2017;23:56–64.

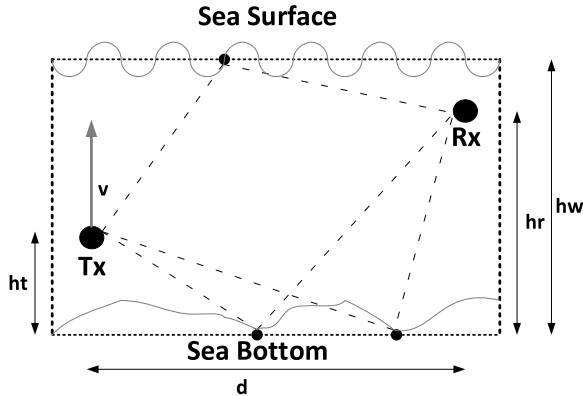


Fig. 19 Simulated Channel Geometry

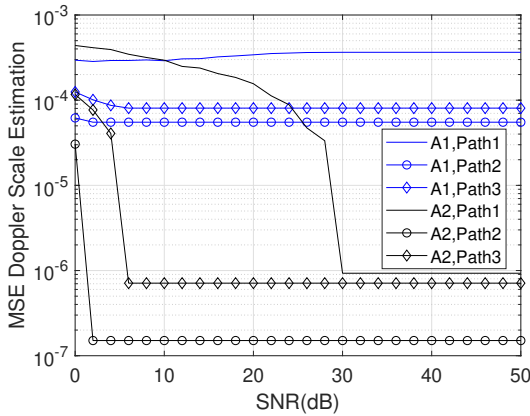


Fig. 20 Performance of the Doppler scale estimation with SNR; A1: wavelet based algorithm [27], A2 : proposed algorithm.

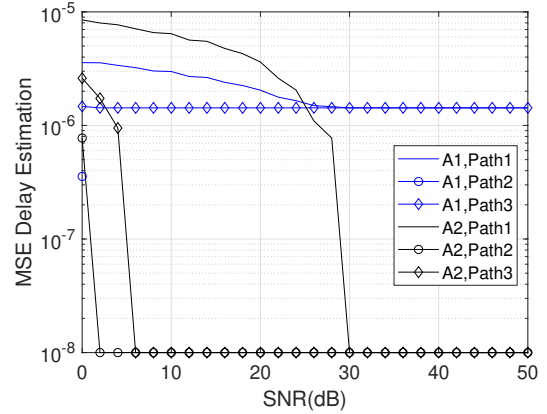


Fig. 21 Performance of the delay estimation with SNR; A1: wavelet based algorithm [27], A2 : proposed algorithm.

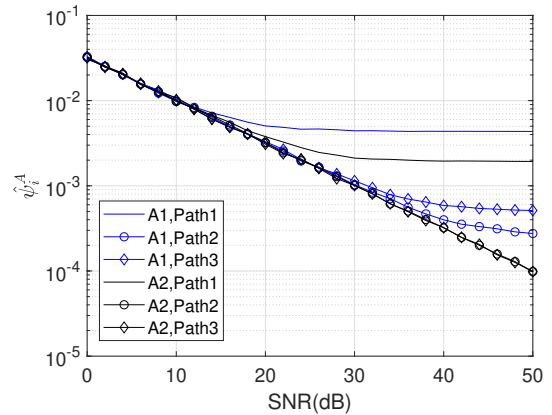


Fig. 22 Performance of the proposed algorithm for channel estimation with SNR: A1: wavelet based algorithm [27], A2 : proposed algorithm.

- [2] Zia MYI, Poncela J, Otero P. State-of-the-Art Underwater Acoustic Communication Modems: Classifications, Analyses and Design Challenges. *Wireless Personal Communications*. 2021;116(2):1325–1360.
- [3] Chitre MA, Potter JR, Ong SH. Optimal and near-optimal signal detection in snapping shrimp dominated ambient noise. *IEEE Journal of oceanic engineering*. 2006;31(2):497–503.
- [4] Mahmood A, Chitre M, Armand MA. PSK communication with passband additive symmetric α -stable noise. *IEEE Transactions on Communications*. 2012;60(10):2990–3000.

- [5] Stojanovic M, Preisig J. Underwater acoustic communication channels: Propagation models and statistical characterization. *IEEE communications magazine*. 2009;47(1):84–89.
- [6] Kochańska I, Schmidt J, Rudnicki M. Underwater acoustic communications in time-varying dispersive channels. In: *2016 Federated Conference on Computer Science and Information Systems (FedCSIS)*. IEEE; 2016. p. 467–474.
- [7] Chen PY, Li HJ. An iterative algorithm for Doppler spread estimation in LOS environments. *IEEE transactions on wireless*

- communications. 2006;5(6):1223–1228.
- [8] Zhao Y, Yu H, Wei G, Ji F, Chen F. Parameter estimation of wideband underwater acoustic multipath channels based on fractional Fourier transform. *IEEE Transactions on Signal Processing*. 2016;64(20):5396–5408.
- [9] Zhang X, Song K, Li C, Yang L. Parameter estimation for multi-scale multi-lag underwater acoustic channels based on modified particle swarm optimization algorithm. *IEEE Access*. 2017;5:4808–4820.
- [10] Li B, Zhou S, Stojanovic M, Freitag L. Pilot-tone based ZP-OFDM demodulation for an underwater acoustic channel. *IEEE*; 2006.
- [11] Lam W, Ormondroyd R. A coherent COFDM modulation system for a time-varying frequency-selective underwater acoustic channel. *IET*; 1997. .
- [12] Zhou Y, Song A, Tong F. Underwater acoustic channel characteristics and communication performance at 85 kHz. *The Journal of the Acoustical Society of America*. 2017;142(4):EL350–EL355.
- [13] Samala R, Deshmukh S. Doppler scaling factor estimation and receiver design for underwater acoustic communication. *Wireless Personal Communications*. 2019;108(4):2415–2433.
- [14] Zhang Y, Xiao S, Liu L, Sun D. 1 0-norm penalized shrinkage LMS algorithm based DFE for underwater acoustic communication. In: 2016 IEEE/OES China Ocean Acoustics (COA). *IEEE*; 2016. p. 1–5.
- [15] Zhang Y, Li J, Zakharov YV, Li J, Li Y, Lin C, et al. Deep learning based single carrier communications over time-varying underwater acoustic channel. *IEEE Access*. 2019;7:38420–38430.
- [16] Wen M, Cheng X, Yang L, Li Y, Cheng X, Ji F. Index modulated OFDM for underwater acoustic communications. *IEEE Communications Magazine*. 2016;54(5):132–137.
- [17] Han J, Zhang L, Zhang Q, Leus G. Eigendecomposition-based partial FFT demodulation for differential OFDM in underwater acoustic communications. *IEEE Transactions on Vehicular Technology*. 2018;67(7):6706–6710.
- [18] Lin CF, Chang SH, Lee CC, Wu WC, Chen WH, Chang KH, et al. Underwater acoustic multimedia communication based on MIMO-OFDM. *Wireless personal communications*. 2013;71(2):1231–1245.
- [19] Liu L, Zhang Y, Zhang P, Zhou L, Li J, Jin J, et al. PN sequence based Doppler and channel estimation for underwater acoustic OFDM communication. In: 2016 IEEE International Conference on Signal Processing, Communications and Computing (ICSPCC). *IEEE*; 2016. p. 1–6.
- [20] Liu C, Zakharov YV, Chen T. Doubly selective underwater acoustic channel model for a moving transmitter/receiver. *IEEE Transactions on Vehicular Technology*. 2012;61(3):938–950.
- [21] Deneire L, Gyselinckx B, Engels M. Training sequence versus cyclic prefix—a new look on single carrier communication. *IEEE Communications Letters*. 2001;5(7):292–294.
- [22] Shen H, Papandreou-Suppappola A. Channel estimation using time-frequency techniques. In: *Proceedings.(ICASSP'05)*. *IEEE International Conference on Acoustics, Speech, and Signal Processing, 2005.. vol. 4*. *IEEE*; 2005. p. iv–513.
- [23] Beygi S, Mitra U. Multi-scale multi-lag channel estimation using low rank approximation for OFDM. *IEEE transactions on signal processing*. 2015;63(18):4744–4755.
- [24] Lin JC. Least-squares channel estimation assisted by self-interference cancellation for mobile pseudo-random-postfix orthogonal-frequency-division multiplexing applications. *IET communications*. 2009;3(12):1907–1918.
- [25] Diamant R, Feuer A, Lampe L. Choosing the right signal: Doppler shift estimation for

underwater acoustic signals. In: Proceedings of the Seventh ACM International Conference on Underwater Networks and Systems; 2012. p. 1–8.

- [26] Berger CR, Zhou S, Preisig JC, Willett P. Sparse channel estimation for multi-carrier underwater acoustic communication: From subspace methods to compressed sensing. *IEEE Transactions on Signal Processing*. 2009;58(3):1708–1721.
- [27] Zhang X, Song K, Li C, Yang L. A novel approach for the estimation of doubly spread acoustic channels based on wavelet transform. *Applied Sciences*. 2018;8(1):38.
- [28] Stojanovic M, Freitag L, Johnson M. Channel-estimation-based adaptive equalization of underwater acoustic signals. In: *Oceans’ 99. MTS/IEEE. Riding the Crest into the 21st Century. Conference and Exhibition. Conference Proceedings (IEEE Cat. No. 99CH37008)*. vol. 2. IEEE; 1999. p. 985–990.
- [29] Chen P, Rong Y, Nordholm S, He Z, Duncan AJ. Joint channel estimation and impulsive noise mitigation in underwater acoustic OFDM communication systems. *IEEE Transactions on Wireless Communications*. 2017;16(9):6165–6178.
- [30] Jiang R, Wang X, Cao S, Zhao J, Li X. Deep neural networks for channel estimation in underwater acoustic OFDM systems. *IEEE access*. 2019;7:23579–23594.
- [31] Sharif BS, Neasham J, Hinton OR, Adams AE. A computationally efficient Doppler compensation system for underwater acoustic communications. *IEEE Journal of oceanic engineering*. 2000;25(1):52–61.
- [32] Swick DA. A review of wideband ambiguity functions. *NAVAL RESEARCH LAB WASHINGTON DC*; 1969.
- [33] Qarabaqi P, Stojanovic M.: Acoustic channel simulator. Tech. Rep.

Appendix A

A.1 Impact of Doppler on LFM signal

Let $l(t)$ be the transmitted LFM signal given by :

$$l(t) = \begin{cases} \cos(2\pi f_0 t + \pi b_l t^2) & 0 \leq t \leq T \\ 0 & \text{otherwise} \end{cases} \quad (\text{A1})$$

where, $b_l = \frac{f_T - f_0}{T}$. b_l is the chirp rate parameter, it indicates the rate of variation of frequency of LFM signal with time. f_T and f_0 be the instantaneous frequency at time $t = T$ and 0 respectively. T is the duration of LFM signal, bandwidth B of LFM signal is given by : $B = |f_T - f_0|$. Consider, channel consisting single path with Doppler scale factor η and with delay of τ , resulting signal is given by:

$$l_\eta(t) = \begin{cases} \sqrt{\eta} \cos(2\pi \eta f_0 t + \pi \eta^2 b_l t^2) & \tau \leq t \leq \frac{T}{\eta} + \tau \\ 0 & \text{otherwise} \end{cases} \quad (\text{A2})$$

After Doppler based scaling:

Instantaneous frequency of both $l(t)$ and $l_\eta(t)$ is w 2given by:

$$f_{lI}(t) = \frac{1}{2\pi} \frac{d}{dt} (2\pi f_0 t + \pi b_l t^2) = f_0 + b_l t \quad (\text{A3})$$

and

$$f_{\eta lI}(t) = \frac{1}{2\pi} \frac{d}{dt} (2\pi \eta f_0 t + \pi \eta^2 b_l t^2) = \eta f_0 + \eta^2 b_l t \quad (\text{A4})$$

respectively. $s_\eta(t)$ has initial instantaneous frequency of ηf_0 at $t = \tau$ and at $t = \frac{T}{\eta} + \tau$ instantaneous frequency is ηf_T .

If LFM signal is Doppler scale invariant, it should result in linear time shift on subjecting to Doppler induced scaling, i.e. :

$$f_{\eta lI}(t) = f_{lI}(t - \Delta t_l). \quad (\text{A5})$$

On substituting, (A3)and (A4) in (A5), we get:

$$\Delta t_l = (1 - \eta^2)t + \frac{1 - \eta}{b_l} f_0. \quad (\text{A6})$$

It shows that the value of Δt_l obtained varies with time.Hence, no fixed value of Δt_l exist for LFM signal.

A.2 Impact of Doppler on HFM signal

Let $s(t)$ be the transmitted HFM signal given by :

$$s(t) = \begin{cases} \cos(\frac{-2\pi}{b} \log(1 - b f_0 t)) & 0 \leq t \leq T \\ 0 & \text{otherwise} \end{cases} \quad (\text{A7})$$

where, $b = \frac{f_T - f_0}{f_T f_0 T}$. b is the chirp rate parameter, it indicates the rate of variation of frequency of HFM signal with time. f_T and f_0 be the instantaneous frequency at time $t = T$ and 0 respectively. T is the duration of

HFM signal, bandwidth B of HFM signal is given by : $B = |f_T - f_0|$.

Consider, channel consisting single path with Doppler scale factor η and with delay of τ , resulting signal is given by:

$$s_\eta(t) = \begin{cases} \sqrt{\eta} \cos\left(\frac{-2\pi}{b} \log(1 - \eta b f_0(t - \tau))\right) & \tau \leq t \leq \frac{T}{\eta} + \tau \\ 0 & \text{otherwise} \end{cases} \quad (\text{A8})$$

After Doppler based scaling:

Instantaneous frequency of both $s(t)$ and $s_\eta(t)$ is given by:

$$f_I(t) = \frac{1}{2\pi} \frac{d}{dt} \left(\frac{-2\pi}{b} \log(1 - b f_0 t) \right) = \frac{f_0}{1 - b f_0 t} \quad (\text{A9})$$

and

$$f_{\eta I}(t) = \frac{1}{2\pi} \frac{d}{dt} \left(\frac{-2\pi}{b} \log(1 - \eta b f_0(t - \tau)) \right) = \frac{\eta f_0}{1 - \eta b f_0(t - \tau)} \quad (\text{A10})$$

respectively. $s_\eta(t)$ has initial instantaneous frequency of ηf_0 at $t = \tau$ and at $t = \frac{T}{\eta} + \tau$ instantaneous frequency is ηf_T . Effective chirp rate factor i.e. b_η is given by :

$$b_\eta = \frac{\eta f_T - \eta f_0}{\frac{T}{\eta} (\eta f_T) (\eta f_0)} = b \quad (\text{A11})$$

which is essentially same that of chirp rate of $s(t)$. Chirp rate governs the shape of time frequency relationship. Hence, HFM pulse retains the shape of time frequency curve even after Doppler induced scaling as a result of that it is invariant to Doppler induced scaling as shown in Fig. A1.

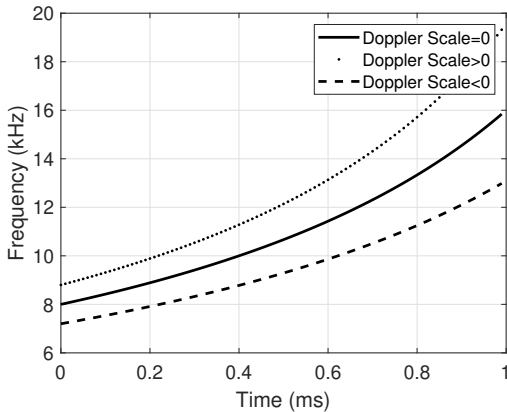


Fig. A1 Scale Invariance of HFM Pulse

Since, HFM chirp signal is Doppler invariant, it means that Doppler induced scaling with factor η of HFM signal will result in linear time shift ΔT . It will satisfy following relationship:

$$f_{\eta I}(t) = f_I(t - \Delta t). \quad (\text{A12})$$

Putting (A9)and (A10) in Equation A12.Value of Δt for up chirp is given by :

$$\Delta t_u = \tau + \frac{1 - \eta}{\eta b f_0}. \quad (\text{A13})$$

Similarly, for down chirp value of Δt is given by:

$$\Delta t_d = \tau - \frac{1 - \eta}{\eta b f_T}. \quad (\text{A14})$$

It indicates that delaying $s(t)$ by Δt will result in signal that is identical of $s(\eta t)$.

Appendix B

HFM signal is Doppler invariant, from (26) and (29), following relationship can be derived:

$$t_u = \tau + \frac{1}{b f_0} \mathbf{\Gamma}^{-1} (\mathbf{\mu} - \boldsymbol{\eta}) \quad (\text{B15})$$

$$t_d = \tau - \frac{1}{b f_T} \mathbf{\Gamma}^{-1} (\mathbf{\mu} - \boldsymbol{\eta}) \quad (\text{B16})$$

where, $\boldsymbol{\tau}$ is a $L \times 1$ vector of propagation delay and Doppler scale factors L multipaths respectively, $\mathbf{\mu}$ is a $L \times 1$ vector containing all ones , $\boldsymbol{\tau} = [\tau_1, \tau_2, \dots, \tau_L]$, $\boldsymbol{\eta} = [\eta_1, \eta_2, \dots, \eta_L]$ and

$$\mathbf{\Gamma} = \text{diag}(\boldsymbol{\eta}) \quad (\text{B17})$$

From (35) and (36) Doppler scaling factor i.e. $\boldsymbol{\eta}$ and channel delay profile i.e. $\boldsymbol{\tau}$ can be estimated as follows:

$$\boldsymbol{\eta} = \Lambda^{-1} T (f_T + f_0) \quad (\text{B18})$$

where, $\Lambda = \text{diag}(T(f_T + f_0) + (\mathbf{t}_u - \mathbf{t}_d)(f_T - f_0))$. Since, $f_T + f_0 = 2f_c$ and $f_T - f_0 = B$, where f_c and B is the centre frequency and bandwidth respectively. (B18) can be written as:

$$\boldsymbol{\eta} = \Upsilon^{-1} \mathbf{\mu} \quad (\text{B19})$$

where, $\Upsilon = \text{diag}\left(\frac{\mathbf{t}_u - \mathbf{t}_d}{T}\right) \left(\frac{B}{2f_c}\right)$.

$$\boldsymbol{\tau} = \frac{\mathbf{t}_u + \mathbf{t}_d}{2} + \frac{T}{2} \mathbf{\Gamma}^{-1} (\boldsymbol{\eta} - 1) \quad (\text{B20})$$